# Supporting Information

## N-doped Graphene-Coated Molybdenum Carbide Nanoparticles as High Efficient Electrocatalyst for Hydrogen Evolution Reaction

Xiaojian Yang, Xiaojia Feng, Huaqiao Tan,* Hongying Zang, Xinlong Wang,* Yonghui Wang, Enbo Wang, and Yangguang Li*

### Contents

## 1. Physical characterization of N-doped $MoC_x$@C-1 and $MoC_x$-2

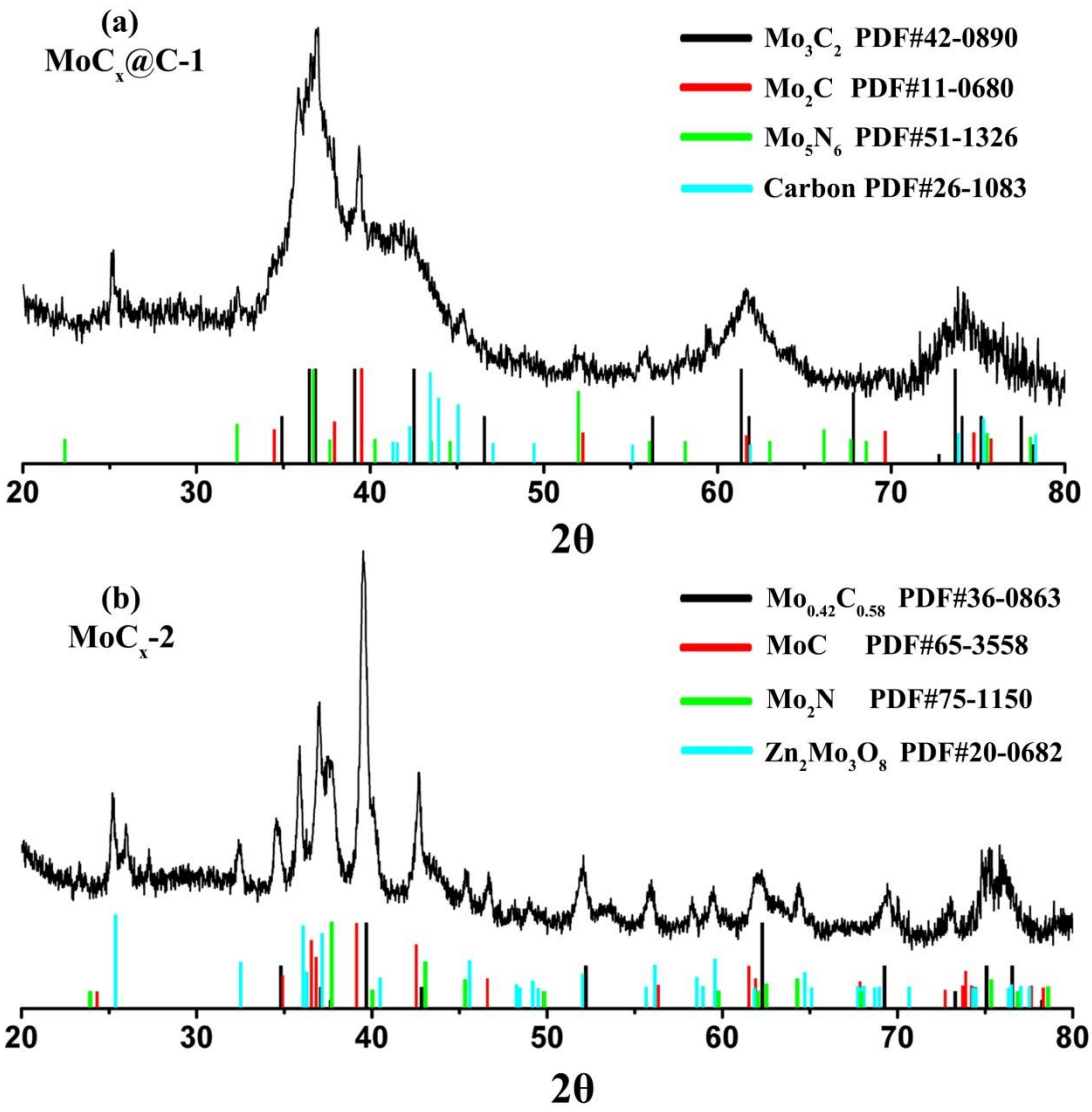


**Fig. S1** X-ray diffraction (XRD) patterns of **$MoC_x$@C-1** and **$MoC_x$-2**. $MoC_x$@C-1 was composed of a mixture of $Mo_3C_2$ (PDF#42-0890), $Mo_5N_6$ (PDF#51-1326), $Mo_2C$ (PDF#11-0680) and carbon (PDF#26-1083). The diffraction peaks of $Mo_5N_6$, $Mo_2C$ and carbon are somewhat masked in the diffraction of $Mo_3C_2$ due to their relatively low crystallinity. As a result, the broadened diffraction peaks are observed in XRD pattern of **$MoC_x$@C-1**. And $MoC_x$-2 was composed of a mixture of $Mo_{0.42}C_{0.58}$ (PDF#36-0863), MoC(PDF#65-3558), $Mo_2N$(PDF#75-1150) and $Zn_2Mo_3O_8$ (PDF#20-0682).

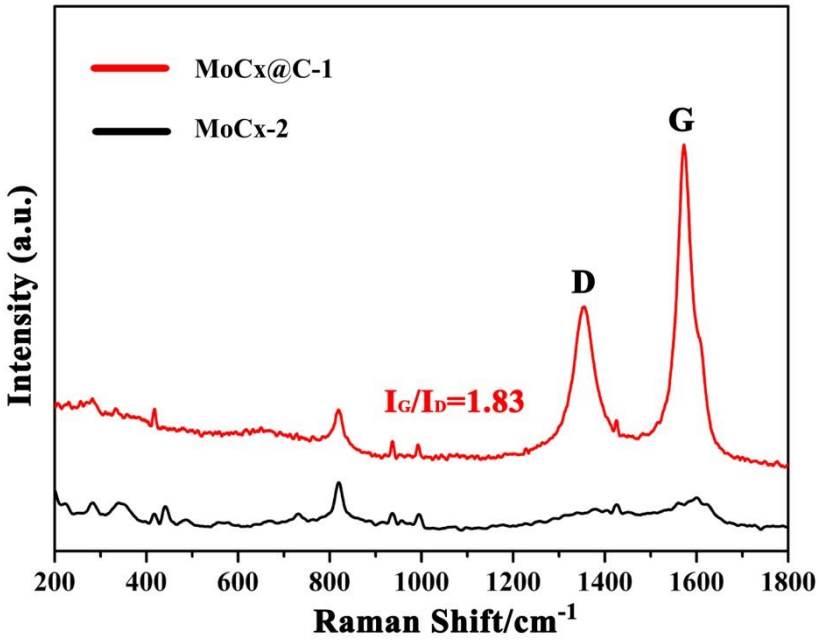


**Fig. S2** The Raman spectra of **$MoC_x$@C-1** and **$MoC_x$-2.** The Raman spectrum of **$MoC_x$@C-1** exhibits two strong peaks at 1350 and 1580 $cm^{-1}$, corresponding to the D and G band of the graphitic carbon. The values of the $I_G/I_D$ were usually applied to judge the graphitization degrees. In this case, the value of $I_G/I_D$ was 1.83, indicating the high graphitization of carbon. The Raman spectrum of **$MoC_x$-2** show no characteristic peaks of carbon. The peaks around 400 and 800 $cm^{-1}$ are attributed to the **$MoC_x$** in both of the **$MoC_x$@C-1** and **$MoC_x$-2.**

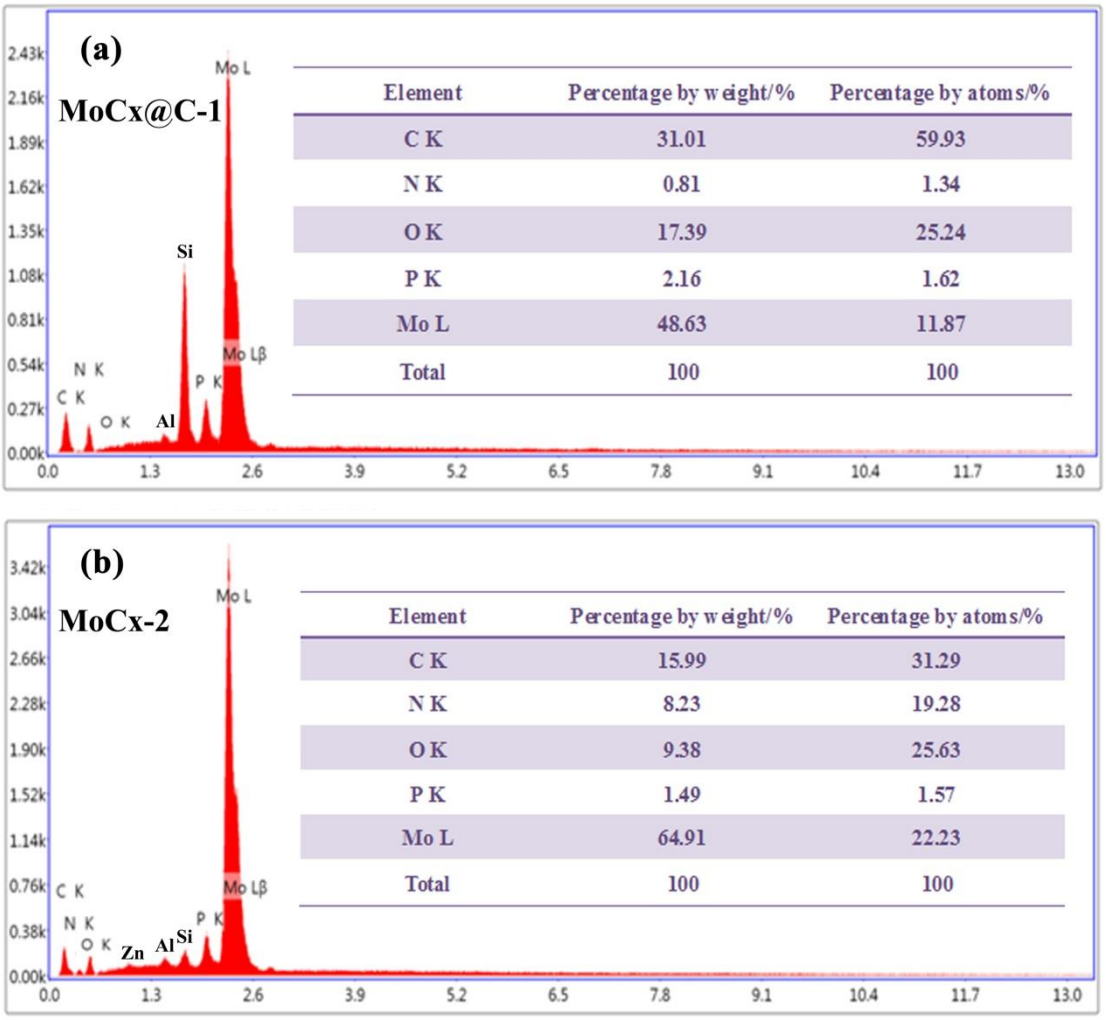


**Fig. S3** The energy dispersive X-ray (EDX) spectra of **MoC$_x$@C-1** and **MoC$_x$-2.** The peaks corresponding to C, N, O, P, Zn and Mo elements (Si and Al peaks originate from the substrate) are observed in both **MoC$_x$@C-1** and **MoC$_x$-2**. The observation of O and P can be assigned to the residual of POMs decomposition. The observed N elements suggest that both **MoC$_x$@C-1** and **MoC$_x$-2** contain N dopants. The carbon content in **MoC$_x$@C-1** was higher than that in **MoC$_x$-2**, which is consistent with the results of TEM results.

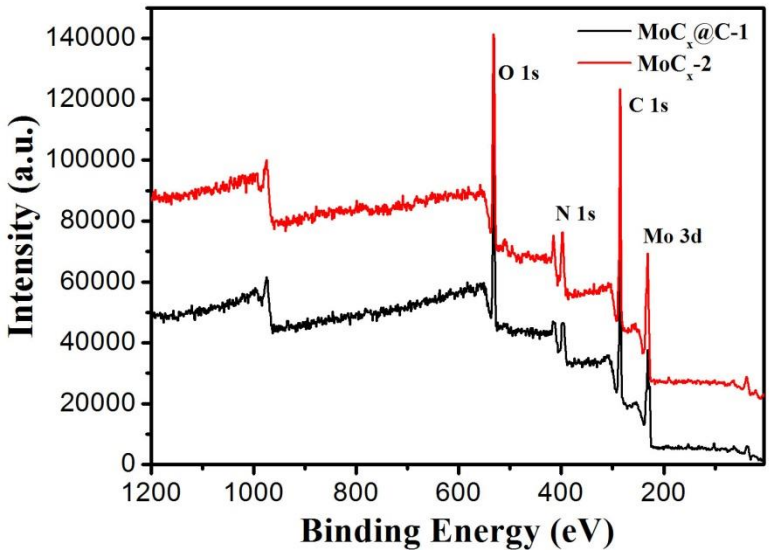


**Fig. S4** X-ray photoelectron spectra (XPS) of **$MoC_x$@C-1** and **$MoC_x$-2.**

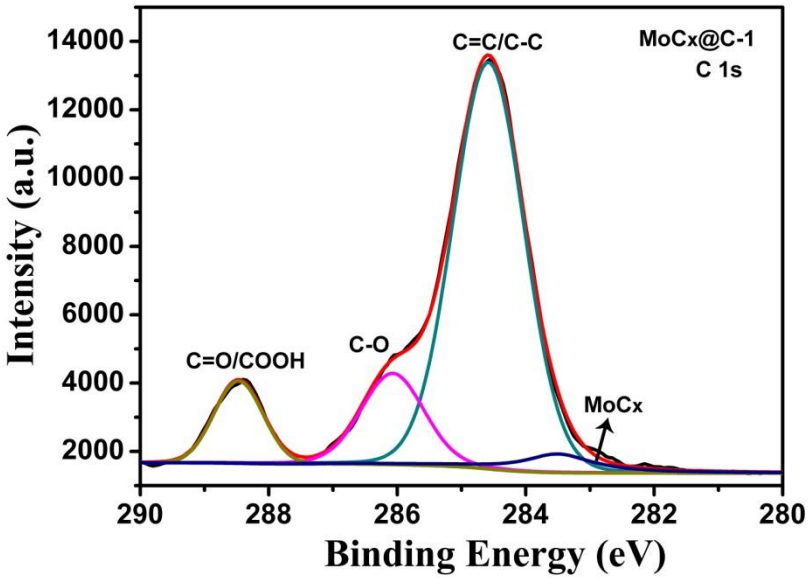


**Fig. S5** The high resolution C 1s XPS of **$MoC_x$@C-1**. The position of the C 1s line of the **$MoC_x$@C-1** attributed to C=C/C-C(284.6 eV) is downshifted by 0.4 eV as compared to that of the GO (285.0 eV), suggesting that the charge transfers in graphene and **$MoC_x$**, which is confirmed with the strong interaction between **$MoC_x$** and rGO [Anwu Xu, J. Mater. Chem. A, 2015, 3, 8055-8061].

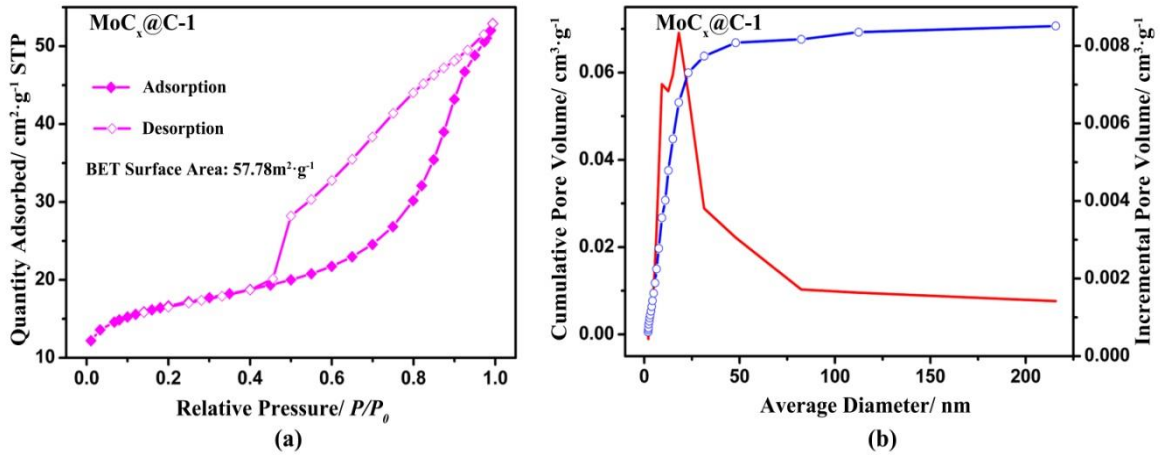


**Fig. S6** The $N_2$ adsorption-desorption isotherms and the pore-size distribution of **$MoC_x$@C-1**.

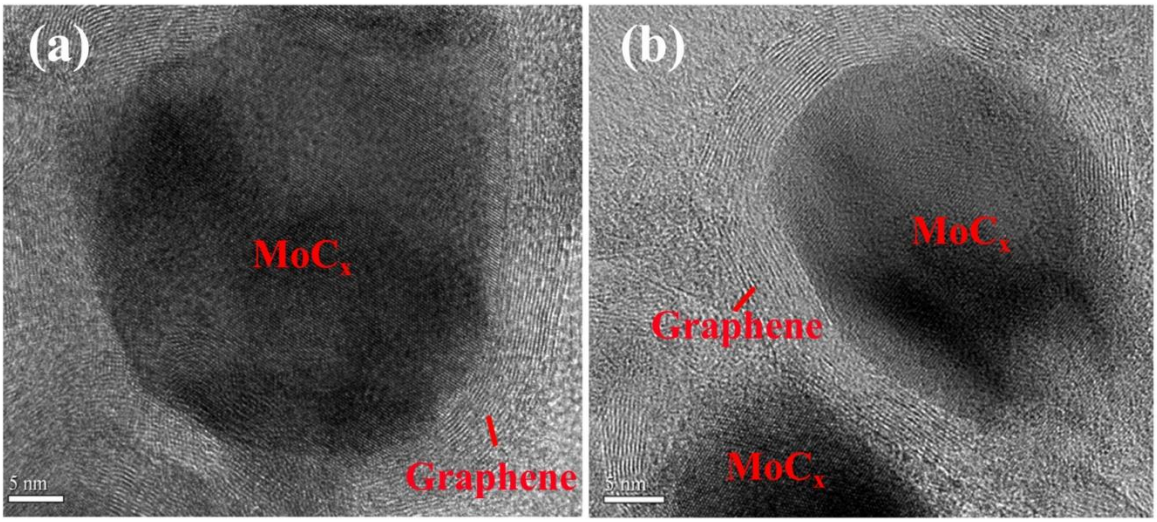


**Fig. S7** The HRTEM images of $MoC_x$@C-1.

## 2. Crystal structures and physical characterization of PECP-1 and PECP-2

### 2.1 Crystallography

Single-crystal X-ray diffraction data for compounds **PECP-1** and **PECP-2** were collected at room temperature 298(2) K with Mo-Kα radiation (λ = 0.71073 Å) by using a Bruker Smart Apex CCD diffractometer and an Oxford Diffraction Gemini R Ultra diffractometer, respectively. All structures were solved by direct methods and refined on $F^2$ by using full matrix least-squares methods in the SHELXTL package.[1] During the refinement of compounds **PECP-1** and **PECP-2**, all non-hydrogen atoms were refined anisotropically, except for the disordered $[Bu_4N]^+$ cations and lattice water molecules in compound **PECP-2**. The hydrogen atoms on organic carbon centers were fixed in calculated positions. Hydrogen atoms on disordered $[Bu_4N]^+$ cations and lattice water molecules cannot be assigned from the weak reflection peaks and were directly included into the final molecular formula. During the refinement, both compounds contain the disordered organic bridging ligands. The bond lengths and bond angles of organic groups were fixed by restraint commands "AFIX 69", "AFIX 59", "DFIX", and "DELU". Furthermore, the restraint commands "ISOR" and "SIMU" were also used to refine these disordered C and N atoms with obvious anisotropic displacement parameters (ADP) and non-positive define (NPD) problems. Moreover, a number of O atoms on POM units were also refined with restraint commands "ISOR" so as to avoid the ADP problems. All above restraint commands led to relatively high restraint values of 141 and 408 in compounds **PECP-1** and **PECP-2**, respectively. The detailed refinement information is listed in the cif files. In the final refinement of compound **PECP-1**, there is still a solvent-accessible void in the compound, but the lattice water molecules cannot be exactly assigned from the weak reflections. Thus, the SQUEEZE program [2] was employed to generate a "SQUEEZE-dry" dataset, which was further used to refine the whole crystal structure. Based on the SQUEEZE calculation results, the elemental analysis, and the TGA,

another two lattice water molecules were directly added to the final molecular formula of compound **PECP-1**. In the refinement of compound **PECP-2**, there is also a solvent-accessible void in the compound. However, the use of SQUEEZE program cannot give a correct "SQUEEZE-dry" dataset. Thus, the extra three lattice water molecules were included in the final molecular formula based on the elemental analysis and TG analysis. Crystal data and structure refinement for compounds **PECP-1** and **PECP-2** are listed in Table S1. Selected bond lengths and angles of **PECP-1** and **PECP-2** are listed in Tables S2–S3 in the Supporting Information. Bond valence sum calculation results of **PECP-2** are listed in Table S4. CCDC 1424108 (**PECP-1**) and 1424109 (**PECP-2**) contain the supplementary crystallographic data for this manuscript. These data can be obtained free of charge from The Cambridge Crystallographic Data Centre via www.ccdc.cam.ac.uk/data_ request/cif.

Reference:

[1] (a) G. M. Sheldrick, *SHELXS-97*, Program for solution of crystal structures, University of Göttingen, Germany, **1997**; (b) G. M. Sheldrick, *SHELXL-97*, Program for refinement of crystal structures, University of Göttingen, Germany, **1997**.

[2] A.L. Spek, *Acta Cryst.* **2009**, *D65*, 148-155.

**Table S1** Crystal data and structure refinement for **PECP-1** and **PECP-2**

| Compounds | **PECP-1** | **PECP-2** |
|---|---|---|
| Formula | $C_{108}H_{88}N_{24}O_{82}P_2Mo_{24}Zn_3$ | $C_{64}H_{84}N_{17}O_{48}PClMo_{13}Zn_3$ |
| *M*r | 5594.63 | 3369.23 |
| T / K | 298(2) | 298(2) |
| Cryst. Syst. | Cubic | Triclinic |
| Space group | *I*a-3d | $P2_1$/m |
| *a*/Å | 31.5350(2) | 13.7949(5) |
| *b*/Å | 31.5350(2) | 18.8786(6) |
| *c*/Å | 31.5350(2) | 19.6726(8) |
| $\alpha$/° | 90 | 90 |
| $\beta$/° | 90 | 105.417(4) |
| $\gamma$/° | 90 | 90 |
| *V*/Å$^3$ | 31360.2(3) | 4938.9(3) |
| *Z* | 8 | 2 |
| $\mu$ / mm$^{-1}$ | 2.419 | 2.444 |
| *F*(000) | 21504 | 3278 |
| Refls collected/unique | 51817 / 2312 | 18380 / 8947 |
| $R_{int}$ | 0.058 | 0.0407 |
| GOF | 1.086 | 1.082 |
| $R_1$ [$I>2\sigma(I)$][a] | 0.0715 | 0.0468 |
| $wR_2$ (all data)[b] | 0.1290 | 0.1295 |

Note: [a]$R_1 = \Sigma||F_o| - |F_c||/\Sigma|F_o|$; [b]$wR_2 = \Sigma[w(F_o^2 - F_c^2)^2]/\Sigma[w(F_o^2)^2]^{1/2}$.

**Table S2** Selected bond lengths (Å) and bond angles (°) of compound **PECP-1.**

| | | | |
|---|---|---|---|
| Mo(1)-O(7) | 1.656(7) | Mo(2)-O(4) | 1.653(8) |
| Mo(1)-O(5) | 1.847(9) | Mo(2)-O(8) | 1.841(7) |
| Mo(1)-O(6) | 1.856(10) | Mo(2)-O(3) | 1.846(8) |
| Mo(1)-O(5)#1 | 1.955(9) | Mo(2)-O(6)#2 | 1.942(9) |
| Mo(1)-O(3) | 1.969(9) | Mo(2)-O(8)#3 | 1.976(7) |
| Mo(1)-O(1)#1 | 2.475(12) | Mo(2)-O(1) | 2.395(13) |
| Mo(1)-O(1) | 2.497(13) | Mo(2)-O(2)#4 | 2.517(12) |
| P(1)-O(2) | 1.46(2) | P(1)-O(1) | 1.571(12) |
| P(1)-O(2)#4 | 1.46(2) | P(1)-O(1)#4 | 1.571(12) |
| P(1)-O(1)#2 | 1.571(12) | P(1)-O(1)#1 | 1.571(12) |
| P(1)-O(1)#3 | 1.571(12) | P(1)-O(1)#5 | 1.571(12) |
| Zn(1)-N(1)#6 | 1.981(5) | Zn(1)-N(1) | 1.981(5) |
| Zn(1)-N(1)#7 | 1.981(5) | Zn(1)-N(1)#8 | 1.981(5) |
| O(7)-Mo(1)-O(5) | 103.2(5) | O(4)-Mo(2)-O(8) | 101.4(4) |

| | | | |
|---|---|---|---|
| O(7)-Mo(1)-O(6) | 103.8(5) | O(4)-Mo(2)-O(3) | 104.6(5) |
| O(7)-Mo(1)-O(5)#1 | 99.8(4) | O(4)-Mo(2)-O(6)#2 | 100.6(5) |
| O(7)-Mo(1)-O(3) | 99.3(4) | O(4)-Mo(2)-O(8)#3 | 98.8(4) |
| O(7)-Mo(1)-O(1)#1 | 158.3(4) | O(4)-Mo(2)-O(1) | 160.6(5) |
| O(7)-Mo(1)-O(1) | 156.4(4) | O(4)-Mo(2)-O(2)#4 | 158.2(5) |
| O(2)-P(1)-O(1)#3 | 112.0(5) | O(2)-P(1)-O(1) | 112.0(5) |
| O(2)-P(1)-O(1)#5 | 112.0(5) | | |
| N(1)#6-Zn(1)-N(1)#7 | 114.5(4) | N(1)#6-Zn(1)-N(1)#8 | 107.03(19) |
| N(1)#6-Zn(1)-N(1) | 107.03(19) | N(1)#7-Zn(1)-N(1)#8 | 107.03(19) |
| N(1)#7-Zn(1)-N(1) | 107.03(19) | N(1)-Zn(1)-N(1)#8 | 114.5(4) |

Symmetry transformations used to generate equivalent atoms: #1 -z+1/2, x+1/2, y; #2 y-1/2, z, -x+1/2; #3 z-1/2, -x+1/2, -y+1; #4 -x, -y+1, -z+1; #5 -y+1/2, -z+1, x+1/2; #6 y-3/4, -x+3/4, -z+1/4; #7 -y+3/4, x+3/4, -z+1/4; #8 -x+0, -y+3/2, z+0.

**Table S3** Selected bond lengths (Å) and bond angles (°) of compound **PECP-2**

| | | | |
|---|---|---|---|
| Mo(1)-O(24) | 1.707(7) | Mo(2)-O(17) | 1.692(4) |
| Mo(1)-O(16) | 1.868(4) | Mo(2)-O(23) | 1.855(5) |
| Mo(1)-O(16)#1 | 1.868(4) | Mo(2)-O(20) | 1.906(4) |
| Mo(1)-O(22)#1 | 1.941(4) | Mo(2)-O(15) | 1.923(3) |
| Mo(1)-O(22) | 1.941(4) | Mo(2)-O(16) | 1.961(5) |
| Mo(1)-O(19) | 2.435(6) | Mo(2)-O(19) | 2.430(4) |
| Mo(3)-O(14) | 1.686(5) | Mo(4)-O(11) | 1.689(5) |
| Mo(3)-O(22) | 1.882(4) | Mo(4)-O(7) | 1.893(5) |
| Mo(3)-O(3) | 1.9076(17) | Mo(4)-O(6) | 1.901(5) |
| Mo(3)-O(21) | 1.913(4) | Mo(4)-O(20) | 1.921(4) |
| Mo(3)-O(6) | 1.929(5) | Mo(4)-O(10) | 1.944(5) |
| Mo(3)-O(18) | 2.424(4) | Mo(4)-O(18) | 2.435(4) |
| Mo(5)-O(9) | 1.662(5) | Mo(6)-O(5) | 1.684(5) |
| Mo(5)-O(21) | 1.917(5) | Mo(6)-O(8) | 1.868(5) |
| Mo(5)-O(7) | 1.928(5) | Mo(6)-O(10) | 1.881(5) |
| Mo(5)-O(12) | 1.934(5) | Mo(6)-O(13) | 1.923(3) |
| Mo(5)-O(4) | 1.9346(18) | Mo(6)-O(23) | 1.983(5) |
| Mo(5)-O(18) | 2.445(4) | Mo(6)-O(2) | 2.437(5) |
| Mo(7)-O(1) | 1.673(7) | Mo(7)-O(8) | 1.968(5) |
| Mo(7)-O(12)#1 | 1.879(5) | Mo(7)-O(8)#1 | 1.968(5) |
| Mo(7)-O(12) | 1.879(5) | Mo(7)-O(2) | 2.426(6) |
| P(1)-O(19) | 1.522(6) | P(1)-O(18) | 1.532(4) |
| P(1)-O(18)#1 | 1.532(4) | P(1)-O(2) | 1.534(7) |
| Mo(8)-O(25) | 1.698(8) | Mo(8)-O(27) | 1.766(5) |
| Mo(8)-O(26) | 1.751(7) | Mo(8)-O(27)#1 | 1.766(5) |

| | | | |
|---|---|---|---|
| Zn(1)-O(26) | 1.980(7) | Zn(2)-N(7) | 1.992(6) |
| Zn(1)-N(1) | 1.995(6) | Zn(2)-N(5) | 1.992(5) |
| Zn(1)-N(1)#1 | 1.995(6) | Zn(2)-N(3)#2 | 2.006(10) |
| Zn(1)-Cl(1) | 2.232(3) | Zn(2)-O(27) | 1.931(5) |
| O(25)-Mo(8)-O(26) | 107.4(4) | O(26)-Zn(1)-N(1) | 100.1(2) |
| O(25)-Mo(8)-O(27) | 109.2(2) | O(26)-Zn(1)-N(1)#1 | 100.1(2) |
| O(25)-Mo(8)-O(27)#1 | 109.2(2) | O(26)-Zn(1)-Cl(1) | 120.0(2) |
| O(27)-Zn(2)-N(7) | 109.5(2) | O(27)-Zn(2)-N(5) | 106.6(2) |
| O(27)-Zn(2)-N(3)#2 | 102.3(3) | | |

Symmetry transformations used to generate equivalent atoms: #1 x, -y+1/2, z; #2 -x+2, -y+1, -z

**Table S4** Bond valence sum calculation results of compound **PECP-2**

| Mo | Mo1 | Mo2 | Mo3 | Mo4 | Mo5 | Mo6 | Mo7 | Mo8 |
|---|---|---|---|---|---|---|---|---|
| BVS[a](R) | 5.92 | 5.93 | 5.98 | 5.89 | 5.87 | 5.94 | 5.90 | 6.13 |
| Analysis | The **average oxidation state** of Mo center on POM: $[R_{Mo1} + 2\times(R_{Mo2} + R_{Mo3} + R_{Mo4} + R_{Mo5} + R_{Mo6})+R_{Mo7}]/12 = [5.92 + 2\times(5.93 + 5.98 + 5.89 + 5.87 + 5.94) + 5.90]/12 = 5.92$ The **average oxidation state** of Mo centers in POM with one Mo(V) and eleven Mo(VI) centers: $(1\times5 + 11 \times 6) /12 = 5.92$ Based on above analysis, it is presumed that there is one reduced Mo(V) center in the $[PMo_{12}O_{40}]^{4-}$ anion in compound **2**, but the reduced electron might be delocalized on the surface oxygen atoms of the POM cluster. | | | | | | | | |

Note: [a]I. D. Brown and D. Altermatt, *Acta Crystallogr., Sect. B: Struct. Sci.*, **1985**, *41*, 244.

### 2.2. Crystal Structure of $[Zn(bimbp)_2]_3[PMo_{12}O_{40}]_2\cdot2H_2O$ (PECP-1)

Single-crystal X-ray diffraction analysis revealed that compound **PECP-1** crystallizes in the cubic space group *I*a-3d. The asymmetric unit contains one-sixth polyoxoanion $[PMo_{12}O_{40}]^{3-}$, a quarter $Zn^{2+}$ atom and a half bimbp ligand (Fig. S8). In **PECP-1**, the polyoxoanion $[PMo_{12}O_{40}]^{3-}$ shows the typical α-Keggin POM structural feature and the central $\{PO_4\}$ group possesses the two-fold disorder. The crystallographically independent Zn1 center is tetra-coordinated by four N atoms derived from four bimbp ligands. The bond length of Zn-N is 1.981(5) Å and the bond angles of N-Zn-N are in the range of 107.03(2)-114.5(4)° (Table S2).

As shown in Fig. S9a, each Zn center is connected with four adjacent Zn centers through the bridging bimbp ligands to form a typically diamond-like coordination framework with Zn…Zn distance of 17.63(1) Å. Interestingly, six of such identical frameworks within the structure form a six-fold interpenetrating framework (Fig. S9b). It is noteworthy that each two interpenetrating diamond-like framework units are parallel with each other and three of such parallel interpenetration groups are further interpenetrated in a declining mode. Usually, the diamond-like coordination framework units tend to multiple parallel interpenetration. In this case, however, one diamond cage is quite large, providing enough space for six-fold declining interpenetration. Furthermore, the Keggin-type polyoxoanions are encapsulated in the void of such host entangled framework (Fig. S9c and S9d) and well isolated by the cationic coordination framework at the molecular level. It is worth mentioning that each diamond cage can contain four Keggin-type POM units, which have never been observed in previously reported POM-encapsulated coordination polymers. Such a structural model can not only uniformly disperse POM clusters but also provide adequate carbon-source surrounded the $[PMo_{12}O_{40}]^{3-}$ anions for carburization and graphitization reaction. Furthermore, the N-donor ligands also provide the opportunity for the introduction of nitrogen dopants into the hybrid molybdenum carbide system.

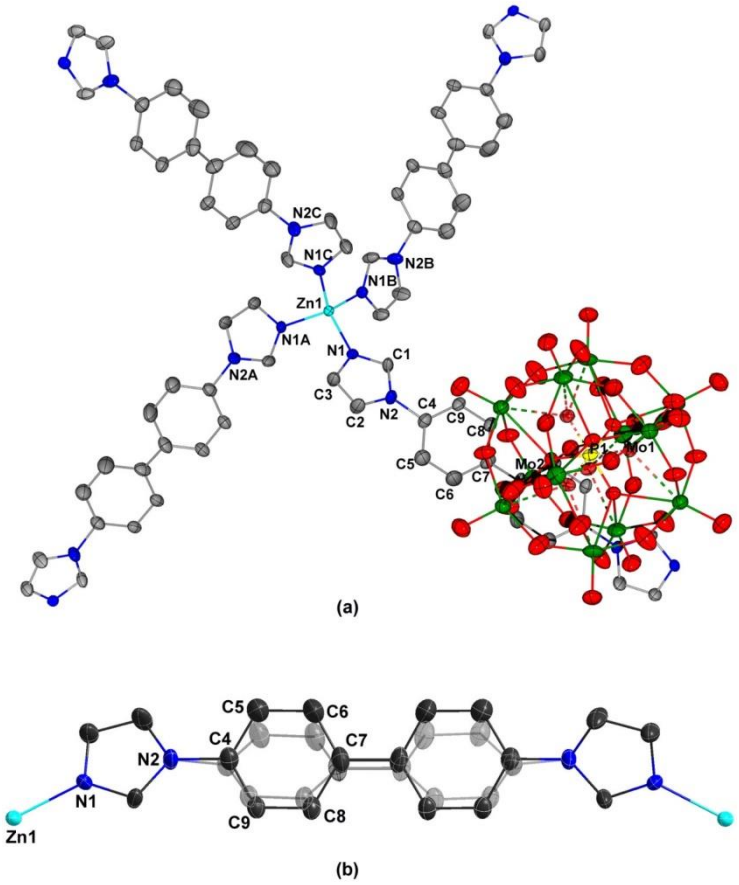


**Fig. S8** ORTEP diagram of **(a)** the structural unit in **PECP-1** with thermal ellipsoids at 30% probability displacement, and **(b)** the disordered ligand in **PECP-1** (Symmetry operation: A: -3/4+y, 3/4-x, 1/4-z; B: 3/4-y, 3/4+x, 1/4-z; C: -x, 3/2-y, z). H atoms are omitted for clarity.

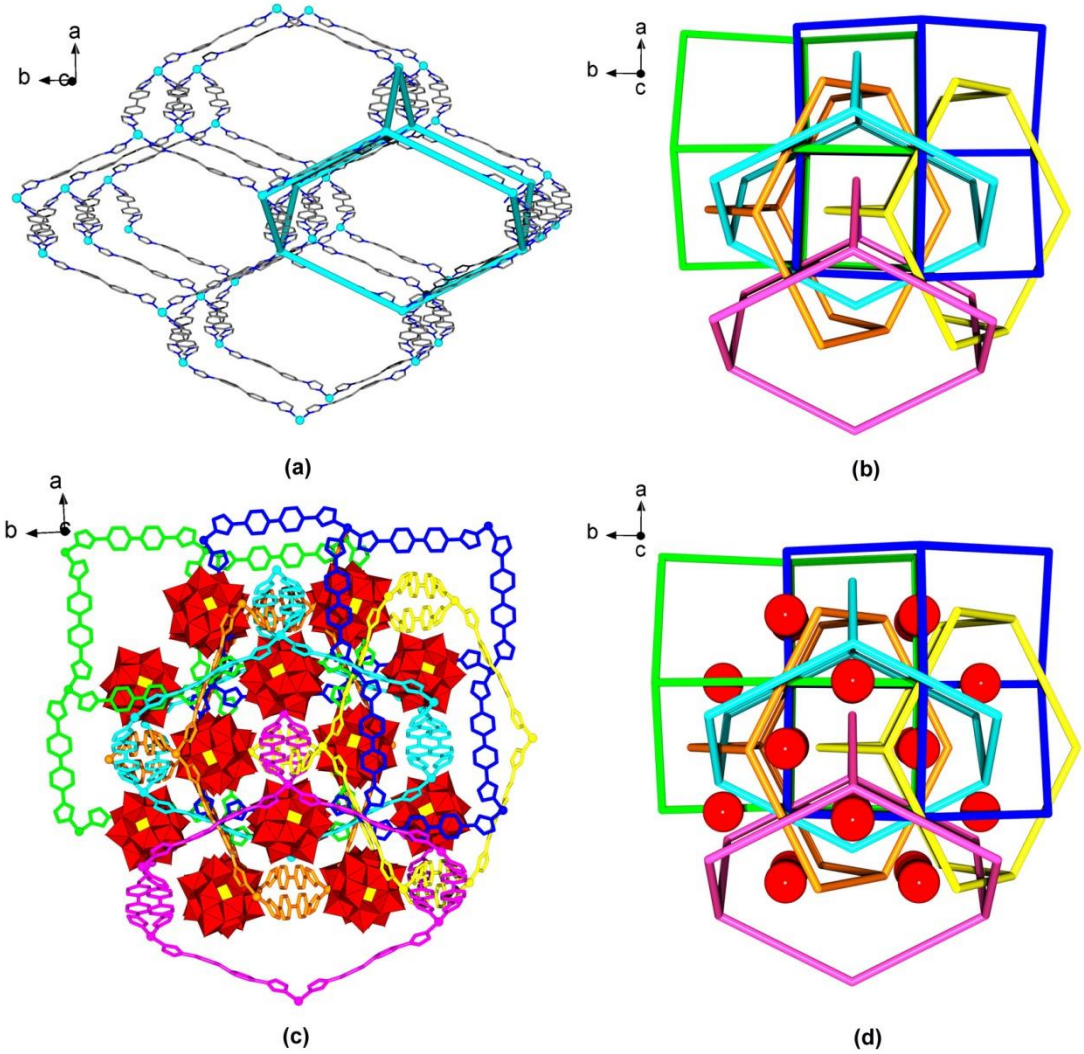


**Fig. S9 (a)** Ball-and-stick view of 3-D diamond-like cationic coordination framework unit in **PECP-1**; **(b)** Schematic view of six-fold interpenetrating diamond-like coordination framework in **PECP-1**; **(c)** Ball-and-stick and polyhedral view of **PECP-1** showing that Keggin-type polyoxoanion guests encapsulated in the entangling cationic framework host. POM units are shown by red polyhedral, and the six interpenetrating diamond-like MOF units are shown by six kinds of colors for clarity; **(d)** Schematic view of an entangled coordination framework encapsulating POM units in **PECP-1**. POM units are shown by red balls, and the diamond-like MOF units are represented by lines with six different colors.

### 2.3. $[Bu_4N][Zn_3(bimb)_4Cl(MoO_4)][PMo^{V}Mo^{VI}_{11}O_{40}]\cdot 4H_2O$ (PECP-2)

Single-crystal X-ray diffraction analysis shows that compound **PECP-2** crystallizes in the monoclinic space group $P2_1/m$. The asymmetric structural unit consists of a half $[PMo^{V}Mo^{VI}_{11}O_{40}]^{4-}$ polyoxoanion, a half $\{MoO_4\}$ fragment, one and a half $Zn^{2+}$ centers, one bimb ligand and two half bimb ligands, and a half $[Bu_4N]^{+}$ cation as well as disordered lattice water molecules (Fig. S10). In the compound **PECP-2**, the $[PMo^{V}Mo^{VI}_{11}O_{40}]^{4-}$ polyoxoanion exhibits the typical Keggin-type structural feature. The oxidation states of Mo centers are confirmed by the black color of the crystalline sample and the bond valence sum (BVS) calculation (Table S4). In the metal-organic coordination moieties, there are two crystallographically independent Zn (Zn1 and Zn2) centers. Zn1 center is four-coordinated with two N atoms derived from two bimb bridging ligands, one terminal $Cl^{-}$ ligand and one O atom derived from $[MoO_4]^{2-}$ anion. Zn2 is also tetra-coordinated with three N atoms derived from three bimb ligands and one O atom derived from $[MoO_4]^{2-}$ anion. Selected bond lengths of Zn-O, Zn-N and Zn-Cl and bond angles of O(N)-Zn-N(O) are listed in Table S3. In compound **PECP-2**, Zn1 and adjacent two Zn2 centers are connected by three bimb bridging ligands to form a triangle ring (Fig. S11a). These triangles are further linked by $[MoO_4]^{2-}$ moieties, forming 1-D double-deck chainlike units along *b* axis (Fig. S11a). Meanwhile, Zn2 centers of adjacent parallel chains are linked by another bimb bridging ligand to give rise to a wavelike 2-D network (Fig. S11a). From the topological viewpoint, all bimb ligands can be considered as linkers, the Mo8 and Zn1 centers can be reduced to three-connected nodes, and the Zn2 centers can be regarded as a four-connected node (Fig. S11b). Thus, the whole network adopts a 3-nodal 3,3,4-c net with stoichiometry (3-c)(3-c)$(4\text{-c})^2$. The point symbol for the net is $\{3.5^2.6^2.7\}_2\{3.6^2\}\{5.6^2\}$. It is noteworthy that such wavelike network form semi-open cavities, each of which is occupied by one Keggin-type polyoxoanion guest (Fig. S11c). In the packing arrangement, these POM-embedded wavelike networks are parallel with each other and the interspaces between two layers are occupied by the $[Bu_4N]^{+}$ cations and lattice

water molecules (Fig. S11d). In this structure, POM clusters are also well dispersed in the coordination networks at the molecular level, which is in favor of uniform carburization and the preparation of nanoscale molybdenum carbide.

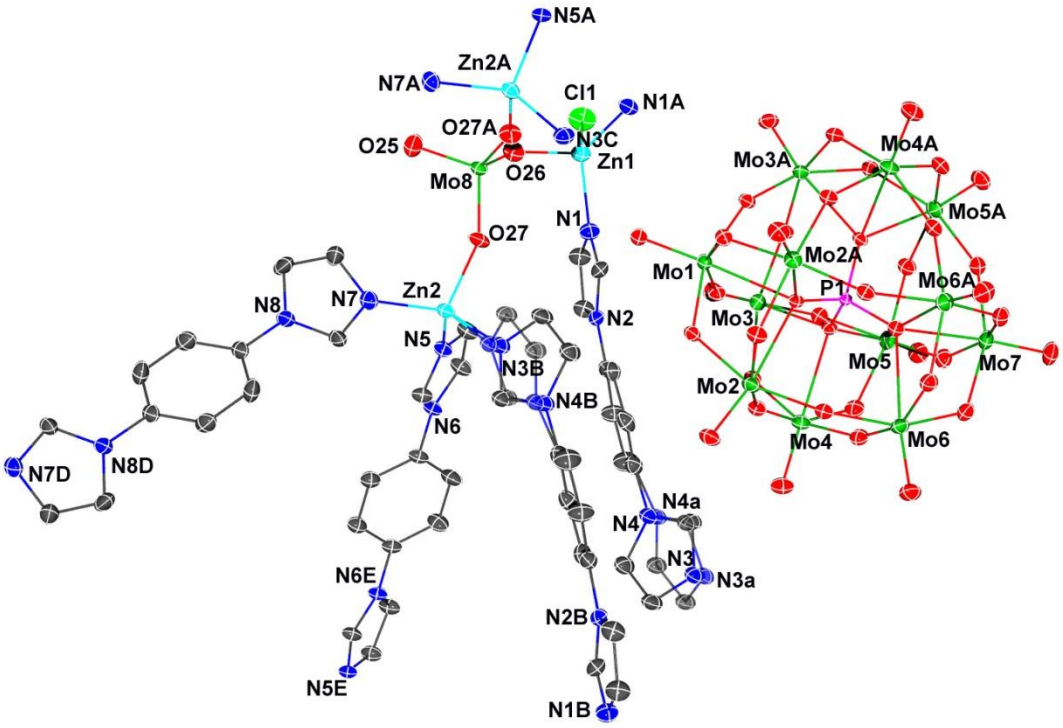


**Fig. S10** ORTEP diagram of the structural unit in **PECP-2** with thermal ellipsoids at 30% probability displacement (Symmetry operation: A: x, 1/2-y, z; B: 2-x, 1-y, -z; C: 2-x, -1/2+y, -z; D: 2-x, 1-y, -1-z; E: x, 3/2-y, z). H atoms are omitted for clarity. The label "a" represent the disordered group in **PECP-2**.

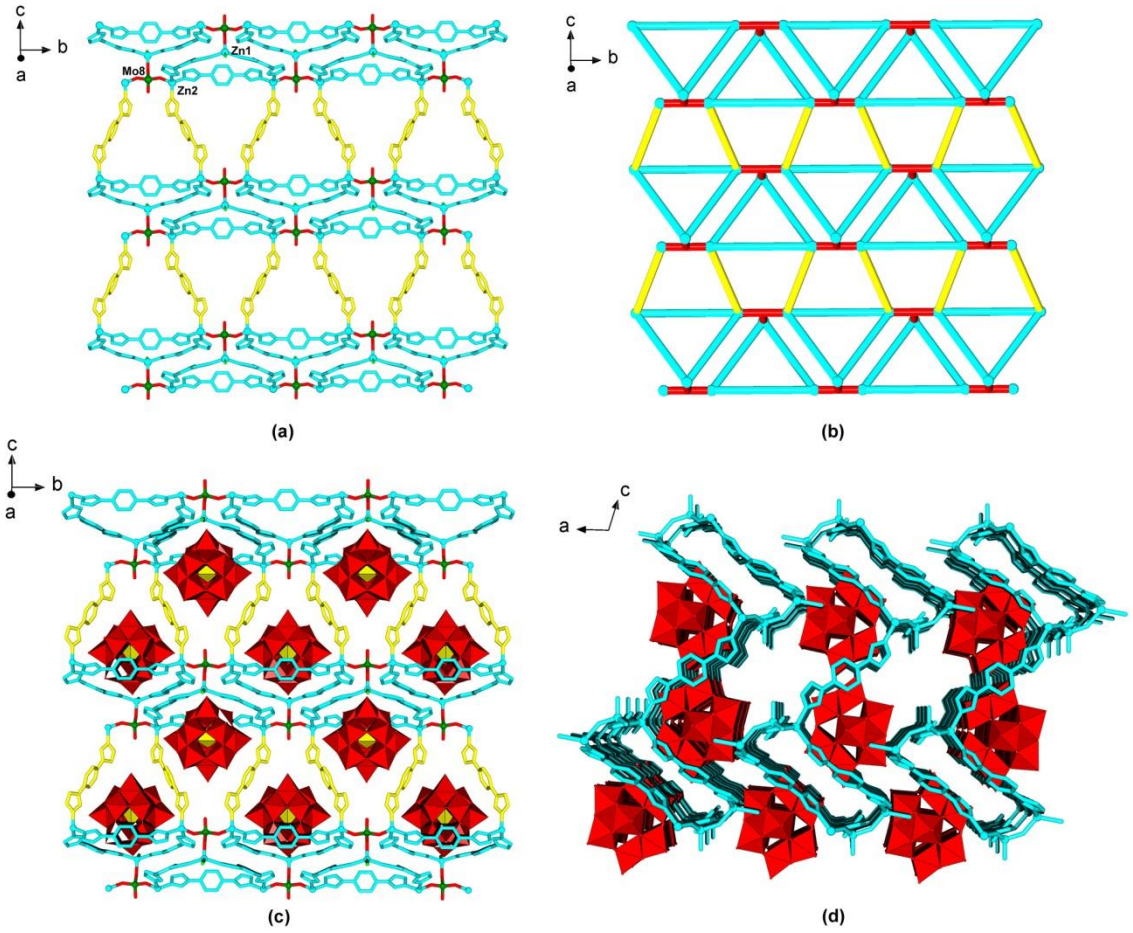


**Fig. S11 (a)** The 2-D wave-like metal-organic coordination network unit in **PECP-2**; **(b)** Schematic view of 2-D layer unit in **PECP-2**. The bimb ligand is represented by line; Zn and Mo centers are represented by blue and red ball, respectively; **(c)** Ball-and-stick and polyhedral view of POM guests residing in the cavity of 2-D network host in **PECP-2**; **(d)** Packing arrangement of **PECP-2** viewed along *b* axis. The $[Bu_4N]^+$ cations and lattice water molecules are omitted for clarity.

## 2.4. Physical characterization of PECP-1 and PECP-2

*TG Analyses:* The TG curve indicates two gradual weight loss steps (Fig. S12a) in the **PECP-1**. The first weight loss, token place in the range of 65~270°C (calcd. 0.70%), is mainly attribute to lose the two lattice water molecules (calcd. 0.64%). The second weight loss ranging from 270 to 730°C is 34.14%, which is mainly attributed to the completely thermal decomposition of the whole **PECP-1**(calcd. 34.48%). The TG curve exhibits two gradual weight loss steps (Fig. S12b) in the **PECP-2**. The first weight loss, occurred in the temperature range of 65~300 °C to be 2.05%, is mainly ascribed to remove the four lattice water molecules (calcd. 2.13%). The second weight loss ranging from 300 to 700 °C is 53.16%, which is mainly attributed to the completely thermal decomposition of the whole **PECP-2**(calcd. 53.06%).

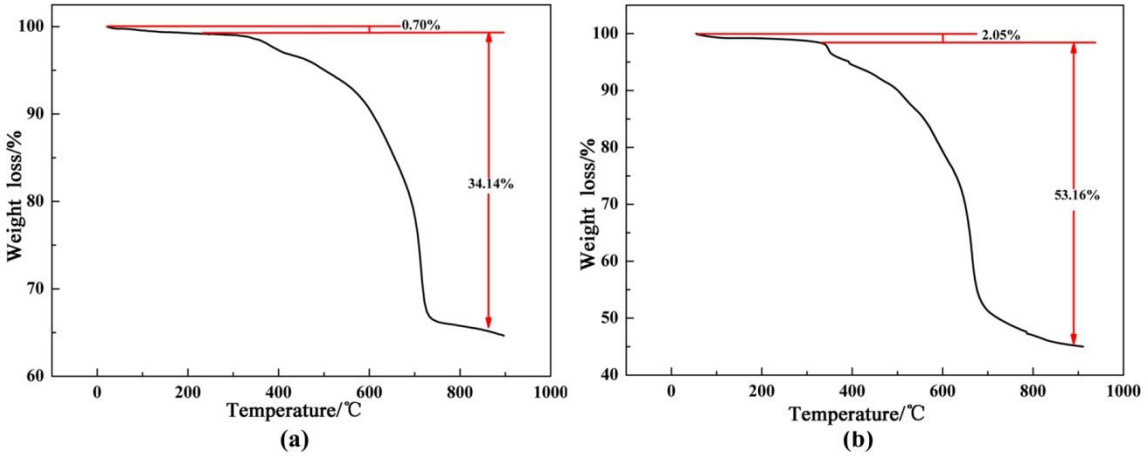


**Fig. S12** (a) The TG curve of **PECP-1**; (b) The TG curve of **PECP-2**.

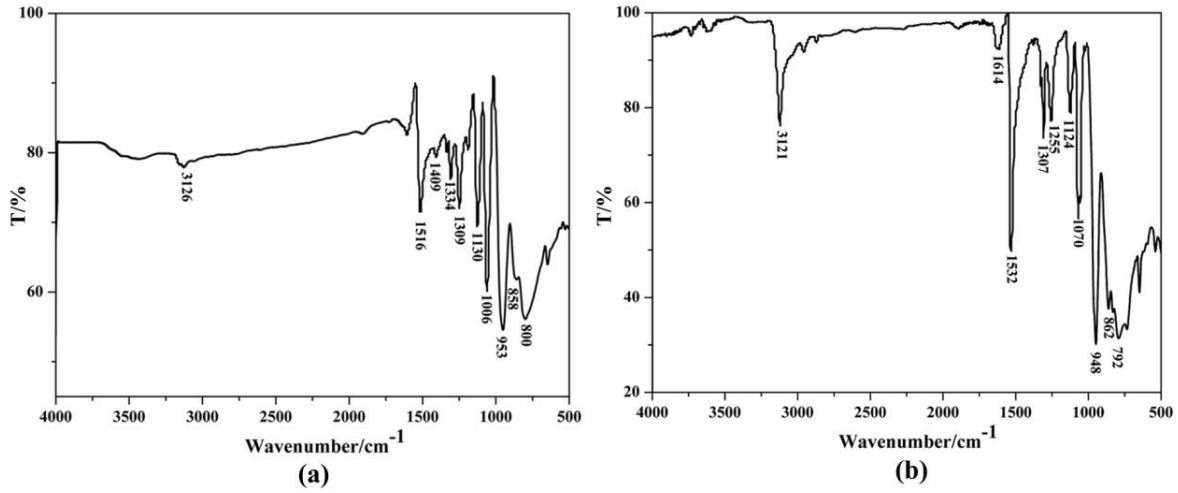


**Fig. S13** IR spectra of **PECP-1** (a) and **PECP-2** (b).

### 3. Additional electrochemical experiments of N-doped $MoC_x$@C-1 and $MoC_x$-2

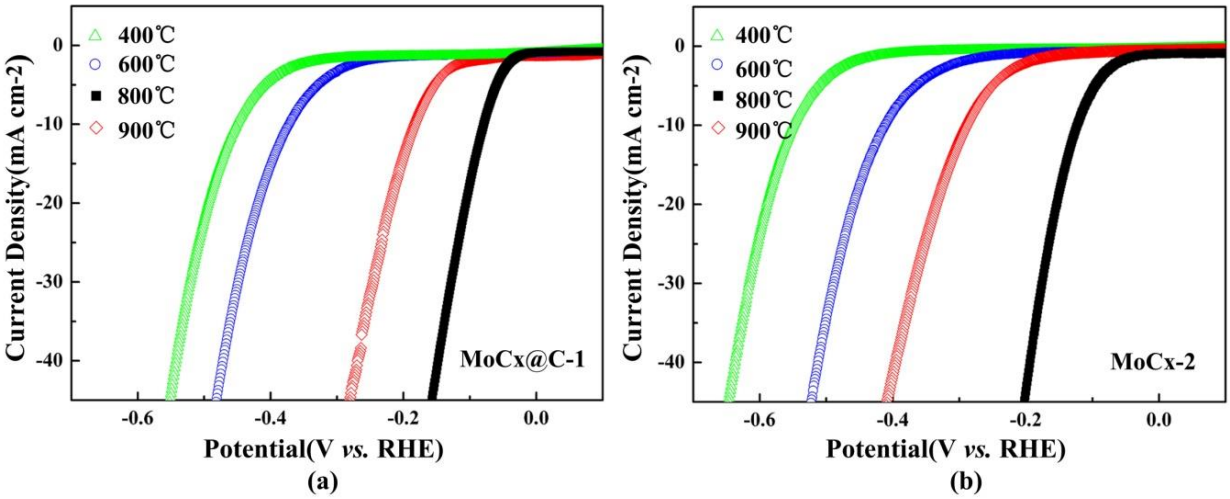


**Fig. S14** Polarization curves of the **$MoC_x$@C-1** and **$MoC_x$-2** at different carburizing temperatures.

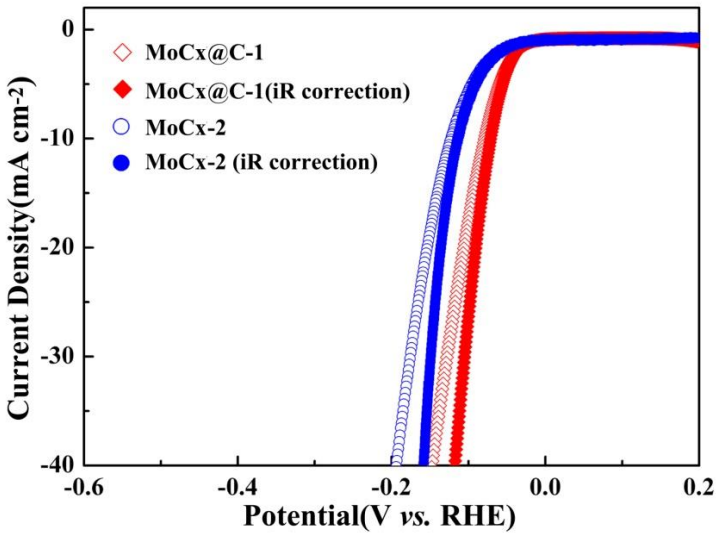


**Fig. S15** Polarization curves of the **$MoC_x$@C-1** and **$MoC_x$-2** after iR correction.

**Table S5** The values of a series resistance ($R_s$) for the **$MoC_x$@C-1** and **$MoC_x$-2** with overpotential from 0.35 to 0.50 V

| | **$MoC_x$@C-1** | **$MoC_x$-2** |
|---|---|---|
| 0.20V | 11.04Ω | 12.90Ω |
| 0.25V | 10.58Ω | 12.45Ω |
| 0.30V | 10.17Ω | 12.05Ω |
| 0.35V | 10.41Ω | 11.89Ω |
| 0.40V | 10.02Ω | 12.38Ω |
| 0.45V | 10.86Ω | 12.76Ω |

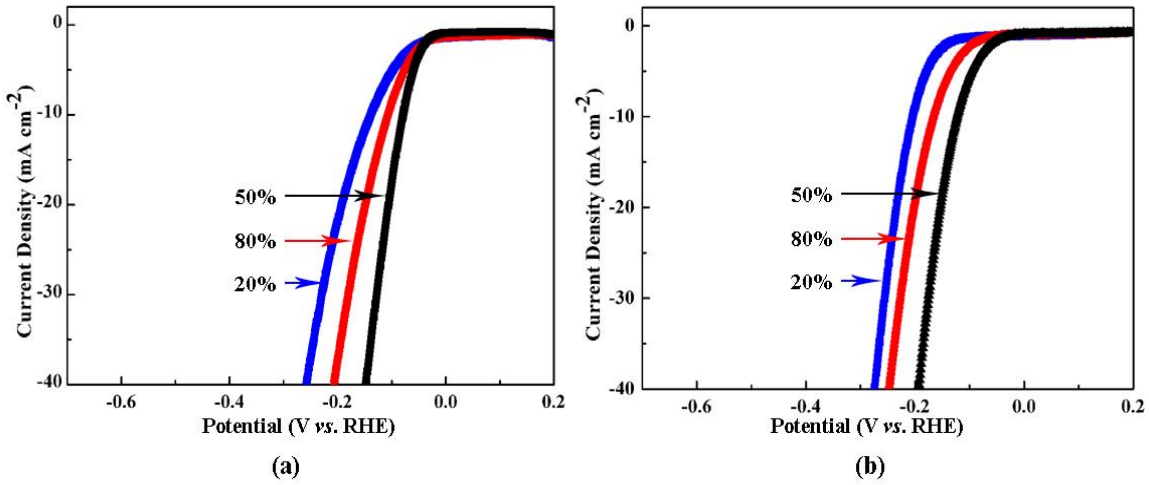


**Fig. S16** Polarization curves of the **$MoC_x$@C-1** and **$MoC_x$-2** with the different mass ratios of the carbon black.

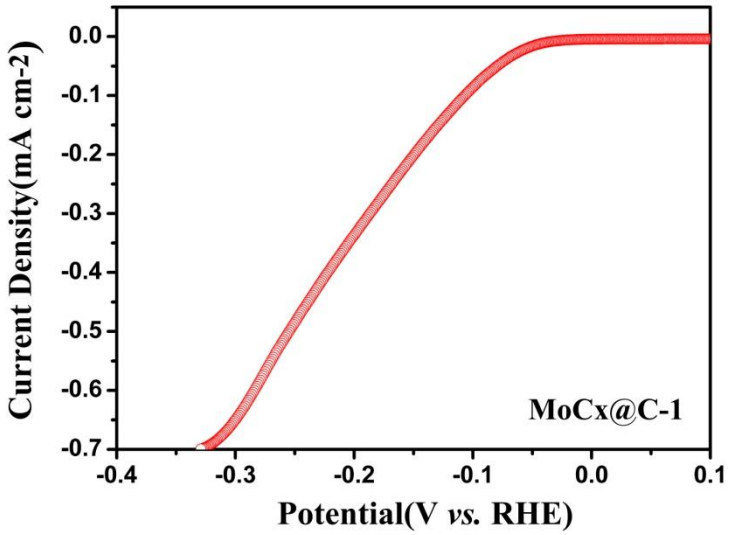


**Fig. S17** Polarization curves of the **$MoC_x$@C-1** with the actual surface area of the HER activity.

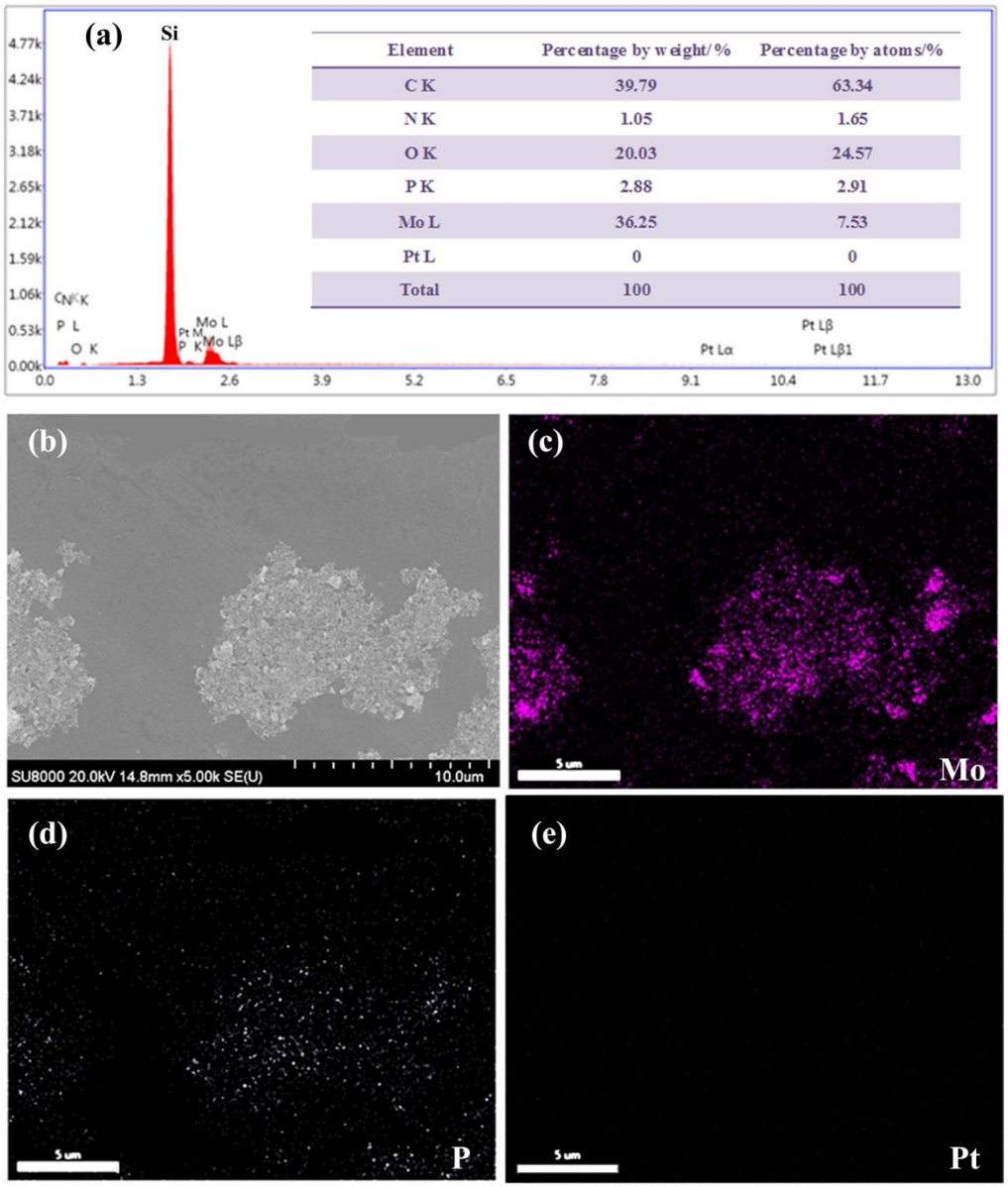


**Fig. S18** (a) The energy dispersive X-ray (EDX) spectra of the sample after HER, (b)-(e) corresponding EDX elemental mapping of Mo, P and Pt in sample after HER.

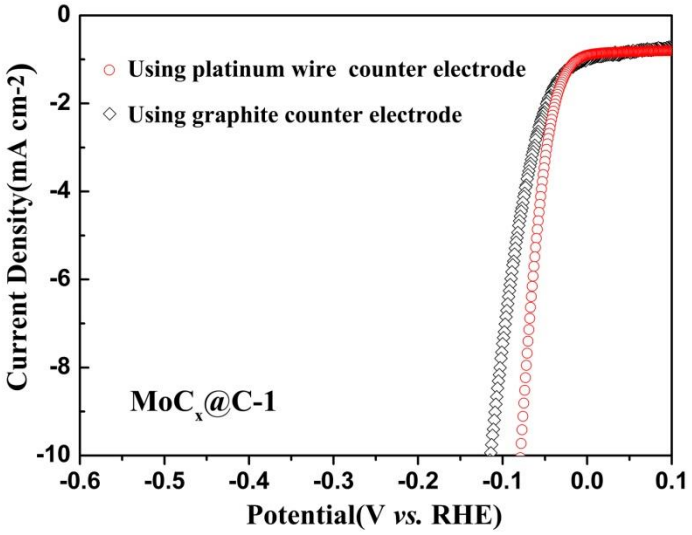


**Fig. S19** Polarization curves of the **$MoC_x$@C-1** by using graphite counter electrode for HER .

## 4. List of HER performance in acid media for reported molybdenum carbide-based electrocatalysts

**Table S6** Comparison of HER performance in acid media for **$MoC_x$@C-1** and **$MoC_x$-2** with other molybdenum carbide-based electrocatalysts

| Catalysts | Onset potential (mV) | Current density (j, mA $cm^{-2}$) | η at corresponding j (mV) | Tafel slope (mV $decade^{-1}$) | Loading of catalyst (mg $cm^{-2}$) | Ref. |
|---|---|---|---|---|---|---|
| **$MoC_x$@C-1** | **21** | **10** | **79** | **56** | **0.354** | **This work** |
| **$MoC_x$-2** | **35** | **10** | **160** | **93** | **0.354** | **This work** |
| Porous $MoC_x$ nano-octahedrons | ∼25 | 10 | 142 | 53 | 0.8 | Ref S1 |
| Porous $Mo_2C$ nano-rod | 68 | 32 | 200 | 58 | 0.43 | Ref S2 |
| $Mo_2C$/GCSs | 120 | 10 | 200 | 62.6 | 0.36 | Ref S3 |
| nw-$W_2MoC$ | — | — | — | 53 | 1.28 | Ref S4 |
| nw-$W_4MoC$ | — | 80 | 184 | 52 | | |
| β-$Mo_2C$ | — | ∼3 | ∼250 | 120 | 0.28 | Ref S5 |
| Bulk $Mo_2C$ | ≥100 | 10 | ∼210 | 56 | 2 | Ref S6 |
| $Mo_2C$–RGO | ∼70 | 10 | ∼175 | ∼57.3 | 0.285 | Ref S7 |
| Np-$Mo_2C$ NWs | 70 | 10 | 130 | 54 | 0.21 | Ref S8 |
| $Mo_2C$–G | 0 | 10 | 150 | 57 | 0.8 | Ref S9 |
| MoC–G | 15 | 10 | 221 | 88 | | |
| $Mo_2C$/CNT | — | 1 | 63 | 55.2 | 30 wt% total Mo metal | Ref S10 |
| | | 10 | 152 | | | |
| $Mo_2C$/XC | | 1 | 105 | 59.4 | | |
| PDAP-MoCN-$CO_2$ | 50 | 10 | 140 | 46 | 0.4 | Ref S11 |
| PDAP-MoCN | 90 | 10 | 190 | 51 | | |
| PANI-MoCN | 120 | 10 | 230 | 50 | | |
| $Mo_2C$-carbon nanocomposites | 100 | 5 | ∼265 | 110-235 | 0.25 | Ref S12 |
| $Mo_2C$/CC | — | 1 | 30 | 124 | 1.5 | Ref S13 |
| | | 10 | 140 | | | |
| P-$Mo_2C$ | — | 1 | 45 | 128 | — | |
| | | 10 | 160 | | | |
| C-$Mo_2C$ | — | 1 | 83 | 168 | | |
| | | 10 | 260 | | | |
| $Mo_2C$ – NCNTs (N-doped carbon nanotubes) | 72 | 1 | 72 | 71 | 3 | Ref S14 |
| | | 10 | 147 | | | |
| α-$Mo_2C$ | — | 10 | 198 | 56 | 0.102 | Ref S15 |
| $Mo_2C$ nanowires | — | 10.2 | 200 | — | — | Ref S16 |
| $Mo_2C$/GR | 150 | 10 | 242 | 82 | 1.4 | Ref S17 |
| $Mo_2C$/CNT –GR | 62 | 10 | 130 | 58 | 0.65 | |
| $Mo_xC$/Ni | — | 10 | ∼150 | — | — | Ref S18 |
| α-$Mo_2C$/CNT | — | 10 | 250 | 251 | 8.2 | Ref S19 |
| α-$Mo_2C$/CXG | — | 10 | 170 | 264 | 6.3 | |

| | | | | | | | |
|---|---|---|---|---|---|---|---|
| Porous 1-D $Mo_2C$–amorphous carbon composites | $Mo_2C$-1 | — | 10 | 134 | 57.5 | ∼3 | Ref S20 |
| | $Mo_2C$-2 | — | 10 | 115 | 57.6 | | |
| | $Mo_2C$-3 | — | 10 | 146 | 74 | | |
| $Mo_2C$/NWs | | — | 10.2 | 200 | 55.8 | 0.357 | Ref S21 |
| $Mo_2C$/ NSs | | — | 5.3 | 200 | 64.5 | | |
| $Mo_2C$@NC | | — | 10 | 124 | 60 | ∼0.28 | Ref S22 |
| $Mo_2C$@NC | | — | 10 | 78 | 41 | 0.25 | Ref S23 |
| $MoO_2P_x$/Mo | | 80 | 10 | 135 | 62 | — | Ref S24 |

**Reference**


[S1] H. B. Wu, B. Y. Xia, L. Yu, X. Y. Yu, X. W. Lou, *Nat. Commun*. **2015**, *6*, 6512-6519.

[S2] P. Xiao, Y. Yan, X. Ge, Z. Liu, J.-Y. Wang, X. Wang, *Appl Catal B- Environ*, **2014**, *154*, 232–237.

[S3] W. Cui, N. Cheng, Q. Liu, C. Ge, A. M. Asiri, X. Sun, *ACS Catal.* **2014**, *4*, 2658−2661.

[S4] P. Xiao, X. Ge, H. Wang, Z. Liu, A. Fisher, X. Wang, *Adv. Funct. Mater.* **2015**, *25*, 1520–1526.

[S5] C. Wan, Y. N. Regmi, B. M. Leonard, *Angew. Chem. Int. Ed.* **2014**, *53*, 6407–6410.

[S6] H. Vrubel, X. Hu, *Angew. Chem. Int. Ed.* **2012**, *51*, 12703–12706.

[S7] L. F. Pan, Y. H. Li, S. Yang, P. F. Liu, M. Q. Yu, H. C. Yang, *Chem. Commun.* **2014**, *50*, 13135–13137.

[S8] L. Liao, S. Wang, J. Xiao, X. Bian, Y. Zhang, M. D. Scanlon, X. Hu, Y. Tang, B. Liu, H. H. Girault, *Energy Environ. Sci.*, **2014**, *7*, 387–392.

[S9] C. He, J. Tao, *Chem. Commun.*, **2015**, *51*, 8323—8325.

[S10] W. F. Chen, C. H. Wang, K. Sasaki, N. Marinkovic, W. Xu, J. T. Muckerman, Y. Zhu, R. R. Adzic, *Energy Environ. Sci.*, **2013**, *6*, 943–951.

[S11] Y. Zhao, K. Kamiya, K. Hashimoto, S. Nakanishi, *J. Am. Chem. Soc.* **2015**, *137*, 110−113.

[S12] N. S. Alhajri, D. H. Anjum, K. Takanabe, *J. Mater. Chem. A*, **2014**, *2*, 10548–10556.

[S13] M. Fan, H. Chen, Y. Wu, L. L. Feng, Y. Liu, G. D. Li, X. Zou, *J. Mater. Chem. A*, **2015**, *3*, 16320–16326.

[S14] K. Zhang, Y. Zhao, D. Fu, Y. Chen, *J. Mater. Chem. A*, **2015**, *3*, 5783–5788.

[S15] L. Ma, L. R. L. Ting, V. Molinari, C. Giordano, B. S. Yeo, *J. Mater. Chem. A*, **2015**, 3, 8361–8368.

[S16] S. Wirth, F. Hamisch, M. Weinmann, U. Schröder, *Appl Catal B- Environ*, **2012**, *126*, 225– 230.

[S17] D. H. Youn, S. Han, J. Y. Kim, J. Y. Kim, H. Park, S. H. Choi, J. S. Lee, *ACS Nano*, **2014**, *8*, 5164 – 5173.

[S18] J. Zhang, X. Meng, J. Zhao, Z. Zhu, *ChemCatChem*, **2014**, *6*, 2059 – 2064.

[S19] B. Šljukić, M. Vujković, L. Amaral, D. M. F. Santos, R. P. Rocha, C. A. C. Sequeira, J. L. Figueiredo, *J. Mater. Chem. A,* **2015**,*3*, 15505–15512.
[S20] K. Zhang, C. Li, Y. Zhao, X. Yu, Y. Chen, *Phys. Chem. Chem. Phys.*, **2015**, *17*, 16609–16614.
[S21] C. Ge, P. Jiang, W. Cui, Z. Pu, Z. Xing, A. M. Asiri, A. Y. Obaid, X. Sun, J. Tian, *Electrochim. Acta*, **2014**, *134* ,182–186.
[S22] Y. Liu, G. Yu, G. D. Li, Y. Sun, T. Asefa, W. Chen, X. Zou, *Angew. Chem. Int. Ed.* **2015**, *54*, 10752 –10757.
[S23] R. G. Ma, Y. Zhou, Y. F. Chen, P. X. Li, Q. Liu, J. C. Wang, *Angew. Chem. Int. Ed.* **2015**, *54*, 14723–14727.
[S24] X. Xie, R. Yu, N. Xue, A. B. Yousaf, H. Du, K. Liang, N. Jiang and A-W. Xu, *J. Mater. Chem. A*, **2016**, *4*, 1647–1652